International Journal of Modeling, Simulation,
and Scientific Computing
Vol. 5, No. 2 (2014) 1350031 (28 pages)

DOI: 10.1142/S1793962313500311

DYNAMICAL MODELING AND CONTROLLABILITY ANALYSIS OF A FLEXIBLE NEEDLE IN SOFT TISSUE

AREFEH BOROOMAND[*,§], MAHDI TAVAKOLI[*,¶],
RON SLOBODA[†,‡,‖] and NAWAID USMANI[†,‡,**]

[*]*Department of Electrical and Computer Engineering*
University of Alberta, Edmonton, AB, Canada T6G 2V4

[†]*Department of Medical Physics, Cross Cancer Institute*
11560 University Avenue, Edmonton, AB, Canada T6G 1Z2

[‡]*Department of Radiation Oncology, Cross Cancer Institute*
11560 University Avenue, Edmonton, AB, Canada T6G 1Z2
[§]*borooman@ualberta.ca*
[¶]*mahdi.tavakoli@ualberta.ca*
[‖]*ron.sloboda@albertahealthservices.ca*
[**]*nawaid.usmani@albertahealthservices.ca*

Received 18 April 2013
Accepted 8 September 2013
Published 3 January 2014

This paper is concerned with deriving a dynamic model of a moderately flexible needle inserted into soft tissue, where the model's output is the needle deflection. The main advantages of the proposed dynamic modeling approach are that the presented model structure involves parameters that are all measurable or identifiable by simple experiments and that it considers the same inputs that are currently used in the clinical practice of manual needle insertion. Conventional manual needle insertion suffers from the fact that flexible needles bend during insertion and their trajectories often vary from those planned, resulting in positioning errors. Enhancement of needle insertion accuracy via robot-assisted needle steering has received significant attention in the past decade. A common assumption in previous research has been that the needle behavior during insertion can be adequately described by static models relating the needle's forces and torques to its deflection. For closed-loop control purposes, however, a dynamic model of the flexible needle in soft tissue is desired. In this paper, we propose a Lagrangian-based dynamic model for the coupled needle/tissue system, and analyze the response of the dynamic system. Steerability (controllability) analysis is also performed, which is only possible with a dynamic model. The proposed dynamic model can serve as a cornerstone of future research into designing dynamics-based control strategies for closed-loop needle steering in soft tissue aimed at minimizing position error.

Keywords: Dynamic modeling; controllability; flexible needle.

1. Introduction

Among several prostate cancer treatment options, permanent implant brachytherapy is considered to be a patient-friendly and minimally invasive surgery with faster recovery time. Brachytherapy involves using needles loaded with radioactive seeds for eliminating cancerous tissue. Once these seed-carrying needles are inserted, they must be steered to reach planned locations in the prostate. After the needle tip reaches the target location, the seeds must be deployed inside the tumor during the process of retracting the needle.

Presently, brachytherapy has emerged as an efficient treatment option for men with localized prostate cancer. Despite good clinical outcomes, brachytherapy's performance is still less than ideal and has room for improvement. In brachytherapy, seed placement is not always done accurately due to various parameters that may change from one patient to the next.

Current practice is that surgeons use a template grid to manually guide needles into the prostate while 2D ultrasound images provide visual feedback about the depth of insertion and if the needle tip is within an acceptable neighborhood of a target position; if not, the surgeon normally retracts the needle partially and re-inserts it for a better result. This procedure assumes that needles remain parallel inside the tissue as they are inserted at different positions in the template grid. However, this is not necessarily the case in reality, causing somewhat significant needle tip positioning errors. Previous work has shown that seeds can be placed at a target position with an average precision of about 5 mm, which is substantial given that the average prostate is only 5 cm in diameter. What is important is that inaccurate needle insertion leads to inaccurate seed placement, which in turn results in delivery of a different radiation dose to the prostate than planned[1,2] and possibly inferior outcomes.[3,4]

With regards to unwanted needle tip misplacement, there are plenty of factors contributing to it. These include the nonlinear behavior of tissue, interaction forces between needle and tissue in directions other than insertion, needle flexibility, prostate deformation and swelling, etc. The most significant factors leading to needle tip misplacement are needle deflection and tissue deformation. Needle deflection is due to the flexibility of the thin needles (clinically popular 18-gauge needles are only 1.27 mm in diameter) used in brachytherapy. There is a coupled relationship between needle deflection and tissue deformation.

A dynamic modeling approach studying the needle/tissue system behavior can help implement computerized needle control strategies for better results in terms of seed placement error. Surveying the literature, the lack of generalized strategies for needle steering using available feedback signals that ensure minimized needle deflection and tissue deformation is evident. It is expected that such strategies yield smaller seed implantation errors than those in manual insertion, meaning that they improve the quality and effectiveness of brachytherapy. For this purpose, i.e., closed-loop control of the needle, real-time feedback of needle deflection and

tissue deformation are necessary besides possibly the estimation of forces/torques acting on the needle.

2. Literature Survey

When a needle is inserted into tissue, modeling needle deflection and tissue deformation is not easy due to the coupling caused by the interaction forces at the interface of the needle and tissue. Needle deflection and tissue deformation are coupled effects. Thus, ideally, needle deflection and tissue deformation modeling should be done with due consideration for this coupling.

2.1. *Rigid needle in soft tissue*

Alterovitz *et al.*[5] assumed a rigid needle and studied the effects of needle tip forces and frictional forces in their simulations. In their research, soft tissue was modeled using a 2D dynamic finite element method. In addition, Dimaio and Salcudean[6] considered a 2D linear elastic model of tissue penetrated by a rigid needle and, based on tissue deformation, calculated needle forces during insertion. Also, Dehghan and Salcudean[7] proposed a new method of path planning for rigid needle insertion into soft tissue. Another soft tissue modeling can be found in Ref. 8.

2.2. *Flexible needle in rigid tissue*

Flexible needles can be categorized into two subgroups, namely highly flexible needles and moderately flexible needles. Webster *et al.*[9] used nonholonomic bicycle and unicycle modeling for steering highly flexible needles. Alterovitz *et al.*[10] steered a flexible needle with a new motion-planning algorithm. Similar to Alterovitz *et al.*,[11] Park *et al.*[12] have also addressed the problem of steering a highly flexible needle through a firm tissue.

2.3. *Flexible needle in soft tissue*

Common needles in brachytherapy are neither completely rigid nor highly flexible. The most common method of modeling this type of needle is the finite element (FE) method.[13] Another approach to model flexible needles is the linear beam theory.[14] Yan *et al.*[15] modeled a needle using linear beam elements. Dehghan *et al.*[16] compared three different models of needle bending including two FE methods, with tetrahedral elements and nonlinear beam elements, as well as an angular spring model.

The aforementioned studies stop short of fully accounting for the coupling between tissue deformation and needle deflection when a flexible needle is inserted into soft tissue. The interaction between a flexible needle and soft tissue during needle insertion is a bilateral phenomenon. The more the tissue is deformed, the more the needle is deflected and vice versa. A few papers have studied this coupled

interaction between needle and tissue during insertion which is difficult to model meticulously although it is important for accurate modeling of the seed placement process.[17] For modeling the soft tissue, a Cauchy strain model was assumed, which leads to a linear relationship between force and displacement. A Green–Lagrange strain model was also studied as a nonlinear model for the force versus displacement relationship.

2.4. *Needle deflection and tissue deformation feedback*

As mentioned before, needle deflection and tissue deformation are known as the two main factors contributing to seed misplacement. There are many ways for measuring these two quantities. The following are methods used in the context of brachytherapy.

For needle deflection measurement, one way is to measure the position of the needle tip directly using a sensor. This method of calculating needle deflection is straightforward and does not need any calculations. However, the cost of this system along with its clinical usability in brachytherapy are causes for concern.

Another technique for needle deflection measurement is to take advantage of image analysis. Among a variety of algorithms, a popular algorithm is the generalized Hough transform,[18] which is a feature extraction technique.

Another existing idea for finding the needle deflection is to use a model of needle deflection in order to relate input variables such as needle base force to needle deflection (i.e., tip position). In general, among these three methods for needle deflection measurement, the image-based algorithm will take the longest and the tracking sensor-based solution will take the shortest time. In addition, image-based algorithms will be less accurate due to imaging limitations but are relatively inexpensive from a hardware perspective.

Similar to the needle deflection measurement, there are different ways to calculate tissue deformation. This quantity can be estimated directly using sensors or indirectly via image processing or tissue modeling. Template matching and morphological methods are common image processing algorithms.

3. Fully Robotic Needle Insertion: Mathematical Modeling

A common assumption in previous research has been that needle behavior during insertion can be adequately described by static models relating the needle's forces and torques to its deflection. We hypothesize that the needle flexibility in soft tissue should also be studied in terms of its transients for closed-loop control purposes. In fact, we hypothesize that enhancing needle insertion accuracy via robot-assisted needle steering may require the knowledge of the dynamical relationship between what causes the deflection and the deflection itself. Therefore, the results in this paper can be regarded as a first step for future research on closed-loop control of flexible needles in soft tissue.

In the following, a Lagrangian-based dynamic model for the coupled needle-tissue system is proposed. Afterwards, steerability (controllability) and observability analyses are performed, which are only possible with a dynamic model. Although inevitably more involved, the proposed dynamic model is expected to be more accurate than static models and to more fully capture the rich dynamics of needle/tissue interaction. To avoid over-complication, we ignore the effect of different tip types (e.g., beveled or trocar) for brachytherapy needles in our modeling. In this paper, we also present system identification for both tissue model and needle/tissue friction model. Simulation results are reported at the end.

3.1. *Previously reported models*

In the literature, there are several studies on modeling of the needle-tissue system using various assumptions. These studies are founded either on the Euler–Bernoulli static beam model or on the dynamic beam model derived from Euler–Lagrange theory.

In Ref. 19, Haddadi *et al.* modeled a needle in soft tissue by considering three external forces at three discrete points. Another model is presented by Lindsey *et al.*,[20] which is derived from Euler–Bernoulli theory.

In Ref. 21, needle deflection is modeled after considering the needle length as consisting of two parts: a part that is inside the tissue and another part that is outside of the tissue.

3.2. *The proposed dynamic model*

In this section, we aim to derive dynamic equations governing a system comprised of a moderately flexible needle inserted in a soft tissue. The proposed dynamic model can serve as a cornerstone of future research into designing dynamics-based control strategies for closed-loop needle steering in soft tissue aimed at minimizing position error.

3.2.1. *Lagrangian formulation*

A general dynamic modeling approach is based on the extended Hamilton's principle. The extended Hamilton's principle for rigid and deformable bodies can be written as the following[22]:

$$\int_{t_1}^{t_2} (\delta T - \delta P) dt + \int_{t_1}^{t_2} \sum_{k=1}^{r} Q_k \delta s_k dt = 0, \tag{1}$$

where $[t_1, t_2]$ is the time interval of motion, δ shows the variation in a parameter, and T and P are the kinetic and potential energies of the system, respectively. In the above, Q_k is the external force in generalized coordinates, δs_k is the vector of corresponding displacements in the same coordinates, and r is the dimension of displacements.

In a conservative system, work done by a force is independent of path, equal to the difference between the final and initial values of an energy function, and completely reversible. If the system we would like to model is conservative, Hamilton's principle will be invariant under coordinate transformations and therefore can be written as

$$\int_{t_1}^{t_2} \delta(T - P)dt = \int_{t_1}^{t_2} \delta L dt = 0. \tag{2}$$

In (2), the *Lagrangian* is defined as the difference between the kinetic and potential energies[23]: $L = T - P$. Applying the variation principle to (2), one can derive the most common representation of Lagrangian-based dynamics as[24]

$$\frac{d}{dt}\left(\frac{\partial L}{\partial \dot{q}}\right) - \frac{\partial L}{\partial q} = F, \tag{3}$$

in which q is the vector of generalized coordinates and F is the vector of corresponding generalized conservative forces.

In the needle and tissue system, we define an inertial and a noninertial coordinate frame (Fig. 1). A noninertial frame has acceleration with respect to an inertial frame. Writing the Lagrangian dynamics in an inertial reference frame is preferable because, if we use a noninertial reference frame, the laws vary from frame to frame depending on the acceleration. For instance, to explain the motion of bodies in a noninertial reference frame, the so-called fictitious forces, which do not arise from any physical interaction, need to be defined in such a way that the motion observed in the noninertial frame is the same as that in the inertial frame. Although sometimes stating a modeling problem in an inertial frame is inconvenient, dealing with fictitious forces in a noninertial frame can be harder. Given the difficulties with noninertial frames, we will use the inertial frame in our system when writing the Lagrangian dynamics of a needle-tissue system.

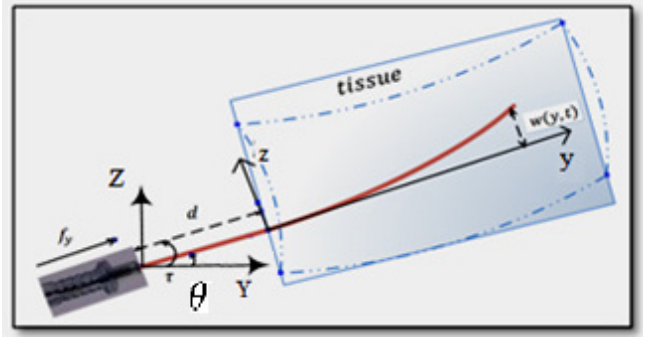

Fig. 1. Schematic of a flexible needle in soft tissue. The origin of the $\{yz\}$ coordinate frame (inertial frame) is the needle entry point into tissue while that of the $\{YZ\}$ frame (noninertial frame) is fixed to the needle base and moves forward as the needle is inserted.

In the needle-tissue system, there are friction forces between the needle and tissue that cannot be neglected in the interaction force. These friction forces make the system nonconservative, and the resulting Hamilton's principle-based equations will be complicated. To avoid this complexity, one can first consider only conservative forces and their corresponding energy equations for writing the Lagrangian dynamics, and then add friction forces directly in the final equations. This approach is used for deriving dynamic models of robots as well.[25]

Disregarding the friction forces, to derive the dynamics of the coupled needle-tissue system, we need to find all of the kinetic and potential energies in the system. Suppose that the flexible needle's base rotates by $\delta\theta$ about an axis perpendicular to the plane of needle deflection and moves forward by a distance δd in the insertion direction — see Fig. 1. For simplicity, we assume that needle deflection and tissue deformation happen only in 2D space, although the following procedure is easily extendable to the case of 3D space.

In Fig. 1, consider the two coordinate frames $\{YZ\}$ and $\{yz\}$ While the former has its origin fixed to the needle base, the latter has its origin at the point of entry of the needle into the tissue, having its y-axis aligned with the unbent needle's axis. Therefore, the $\{yz\}$ frame, which is in inertial motion, is considered as the reference frame in this study. In Fig. 1, $w(y,t)$ denotes the needle's deflection as a function of time and space. Also, f_y and τ are the force and torque (applied by the robot or manually) along the y-axis and around the x-axis (found from completing the $\{yz\}$ frame using the right-hand rule), respectively.

Assumptions. The following is a list of simplifying assumptions used in this modeling:

(1) Needle insertion and deflection are in a 2D plane that is perpendicular to the gravity vector.
(2) Needle bending outside the tissue is negligible in comparison with that inside the tissue.
(3) Torsional deflection of the needle can be neglected.
(4) The effects of needle bevel tip on needle deflection can be neglected.
(5) A model of tissue is homogeneous without considering swelling phenomena.
(6) Flexible needle has a constant linear density ρA, a constant Young's modulus E, and constant area moments of inertia I_y and I_x.

Generally, the kinetic energy of a body is found as

$$T(t) = \int_{\text{along body}} \hat{T}(y,t)dy,$$

where $\hat{T}$ is the kinetic energy density. Using the predefined generalized coordinate system, any point on the needle can be specified in the $\{yz\}$ frame by three variables $d, w(t,y)$ and y, which are the length of needle outside of tissue, the needle's deflection along its length, and the needle point's coordinate along the y-axis,

respectively. The quadratic form of the needle's kinetic energy is

$$T = \frac{1}{2}\int_{-d}^{l-d} \rho A \dot{s}^T \dot{s} dy, \tag{4}$$

where ρ is the density, A is the effective cross-sectional area, and l is the total needle length (comprised of the needle segments inside and outside the tissue). Also, s is the position vector of any point on the needle, which is split into s_1 (for needle points outside the tissue) and s_2 (for needle points inside the tissue).

Given the above-mentioned assumptions, the coordinates of a point on the needle can be written as follows. For the sake of brevity, we have denoted the needle's deflection $w(t, y)$ by w.

$$s = \begin{cases} s_1 = \begin{bmatrix} y \\ 0 \end{bmatrix}; & -d < y \ll 0 \\ s_2 = \begin{bmatrix} y \\ w \end{bmatrix}; & 0 < y < l - d \end{cases},$$

$$\dot{s} = \begin{cases} s_1 = \begin{bmatrix} \dot{y} \\ 0 \end{bmatrix}; & -d < y \ll 0 \\ s_2 = \begin{bmatrix} \dot{y} \\ \dot{w} \end{bmatrix}; & 0 < y < l - d \end{cases},$$

where from Fig. 1, d is the length of the needle outside of the tissue. Substituting the above $\dot{s}$ in (4) leads to the following linear kinetic energy for the needle:

$$\begin{aligned} T_L &= \frac{1}{2}\int_{-d}^{0} \rho A \dot{s}_1^T \dot{s}_1 dy + \frac{1}{2}\int_{0}^{l-d} \rho A \dot{s}_2^T \dot{s}_2 dy \\ &= \frac{1}{2}\int_{-d}^{0} \rho A \dot{y}^2 dy + \frac{1}{2}\int_{0}^{l-d} \rho A (\dot{y}^2 + \dot{w}^2) dy. \end{aligned} \tag{5}$$

We can split the above kinetic energy into two terms, namely T_{L1}, the kinetic energy related to the axial and rotational movements of the needle's rigid body, and T_{L2}, the kinetic energy corresponding to the needle's flexibility. It is easy to show that

$$T_{L1} = \frac{1}{2}\int_{-d}^{l-d} \rho A (\dot{y}^2) dy = \frac{1}{2}\rho A l \dot{y}^2,$$

$$T_{L2} = \frac{1}{2}\int_{0}^{l-d} \rho A (\dot{w}^2) dy.$$

In addition to T_L, the rotational kinetic energy of the needle is calculated by

$$T_R = \frac{1}{2}\int_{0}^{\dot{\theta}} I_x \dot{\theta} d\dot{\theta} = \frac{1}{4} I_x \dot{\theta}^2.$$

The potential energy of the needle/tissue system changes as the tissue deforms. This energy generally varies due to three effects: gravity, needle elasticity, and tissue deformability. In our system, gravity does not have any effect on the potential

energy of the system since the plane of needle insertion and deflection is assumed to be parallel to the ground. The potential energy stored in needle elasticity is[26]:

$$P_{ne} = \frac{1}{2}\int_0^{l-d} EI_y \left(\frac{\partial^2 w}{\partial y^2}\right)^2 dy. \tag{6}$$

where E is the Young's modulus and I_y is the cross-sectional moment of inertia of the needle. Also, one can write the potential energy stored in the deformed tissue as

$$P_{td} = \int_0^{l-d} \left(\int k(d,t)w(y,t)dw\right) dy, \tag{7}$$

in which $k(d,t)$ is the stiffness coefficient of the spring mesh that models the soft tissue. The dependence of k on d accounts for tissue non-homogeneities, and its variation with time t allows simulation of *in vivo* reaction (such as swelling) of sensitive tissues in response to the applied forces. Considering fifth assumption,

$$k(d,t) = k_a = \text{const.} \tag{8}$$

In (7), the tissue model will become even simpler after considering one equivalent spring connected at the needle's tip.

Overall, the Lagrangian can be calculated from (5)–(8) as

$$\begin{aligned} L = {} & \frac{1}{2}\rho A l\dot{y}^2 + \frac{1}{2}\int_0^{l-d} \rho A(\dot{w}^2)dy + \frac{1}{4}I_x\dot{\theta}^2 \\ & - \frac{1}{2}\int_0^{l-d} EI_y \left(\frac{\partial^2 w}{\partial y^2}\right)^2 dy - \frac{1}{2}(k_a)\int_0^{l-d} \left(\int w dw\right) dy. \end{aligned} \tag{9}$$

For tractability of the derivation of the coupled needle-tissue Lagrangian dynamic model, we make two additional common assumptions. With respect to assumption 6, ρA and EI_y can be moved outside the integrals. It is generally agreed that this assumption is not far from reality.

Second, in (9), the Lagrangian depends on the deflection $w(y,t)$, which is a function of two variables: time and space. The well-known *assumed mode* method makes the assumption that two-variable deflection function can be approximated by separable one-variable functions of time and space. See Ref. 27 for more details. Using *assumed mode* method, deflection can be expressed as,

$$w(y,t) = \lim_{n\to\infty} \sum_{i=1}^{n} q_i(t)\varphi_i(y) \approx q_1(t)\varphi_1(y) + q_2(t)\varphi_2(y), \tag{10}$$

where $\varphi_i(y)$ is a vector of n "shape modes" and $q_i(t)$ is the corresponding vector of generalized coordinates. This means that a continuous deflection is approximated by an infinite series composed of products of time-dependent and space-dependent functions.

In this study, to limit the complexity and dimension, two dominant first modes are considered. The shape mode $\varphi_i(y)$ has the following general structure obtained through the Euler–Bernoulli beam equation[28]:

$$\varphi_i(y) = c_i[(\sin(k_i y) - \sin h(k_i y))] - \frac{\sin(k_i l) + \sin h(k_i l)}{\cos(k_i l) + \cos h(k_i l)}(\cos(k_i y) + \cos h(k_i y)), \tag{11}$$

in which k_i can be computed by solving $\cos(k_i l)\cos h(k_i l) + 1 = 0$. Defining μ as

$$\mu = \frac{\sin(k_i l) + \sin h(k_i l)}{\cos(k_i l) + \cos h(k_i l)}.$$

$\varphi_i(y)$ is reduced to

$$\varphi_i(y) = c_i[(\sin(k_i y) - \sin h(k_i y))] - \mu(\cos(k_i y) + \cos h(k_i y)),$$

in which c_i is a normalizing constant found such that the equation below is satisfied.

$$\int_0^l ((\varphi_i(y))^2 dy = 1.$$

Simplifying the above for finding coefficients c_i leads to

$$\frac{2\mu}{k_i}\sin(k_i l)\sin h(k_i l) + \frac{1}{k_i}(1-\mu^2)\cos(k_i l)\sin h(k_i l) - \frac{1}{k_i}(1+\mu^2)\sin(k_i l)\cos h(k_i l) + \frac{1}{4k_i}(1+\mu^2)\sin h(2k_i l) + \frac{1}{4k_i}(\mu^2-1)\sin(2k_i l) + \frac{\mu}{2k_i}(\cos(2k_i l) - \cos h(2k_i l)) + \mu^2 l = \frac{1}{c_i^2}.$$

Consequently, (9) can be rewritten as (12) where a prime denotes differentiation with respect to the space variable y (whereas a dot denotes differentiation with respect to the time variable t):

$$L = \frac{1}{2}\rho A l\dot{y}^2 + \frac{1}{2}\rho A\dot{q}_1^2\int_0^{l-d}\varphi_1^2(y)dy + \frac{1}{2}\rho A\dot{q}_2^2\int_0^{l-d}\varphi_2^2(y)dy + \rho A\dot{q}_1\dot{q}_2\int_0^{l-d}\varphi_1(y)\varphi_2(y)dy + \frac{1}{4}I_x\dot{\theta}^2 - \frac{1}{2}EI_y q_1^2\int_0^{l-d}(\varphi_1'')^2 dy - \frac{1}{2}EI_y q_2^2\int_0^{l-d}(\varphi_2'')^2 dy - EI_y q_1 q_2\int_0^{l-d}\varphi_1''\varphi_2'' dy - \frac{1}{2}k_a q_1^2\int_0^{l-d}\varphi_1^2(y)dy - \frac{1}{2}k_a q_2^2\int_0^{l-d}\varphi_2^2(y)dy - k_a q_1 q_2\int_0^{l-d}\varphi_1(y)\varphi_2(y)dy. \tag{12}$$

To substitute the above in (3), we note that q and F are

$$q = \begin{bmatrix} d \\ \theta \\ q_1 \\ q_2 \end{bmatrix}, \quad F = \begin{bmatrix} f_y \\ \tau \\ 0 \\ 0 \end{bmatrix},$$

where from Fig. 1, d is the length of needle outside of the tissue and θ is the deflection angle. q_i is the vector of generalized coordinates. It is obvious that the two external forces, f_y and τ, are applied along the y-axis and around the x-axis, respectively. Since no external force is applied along the z-axis (i.e., in the direction of q_1 and q_2), the last two rows of F are zero. Also, we note that $\dot{y} = \dot{d}$. Substituting (12) into (3) followed by simplification and rearrangement of the resulting terms yields the nonlinear dynamic equation of the needle in the tissue (excluding nonconservative forces) in the general form of Eq. (13).

$$M(q)\ddot{q} + N(q, \dot{q}) = F. \tag{13}$$

Here, $M(q)$ is a 4×4 matrix in terms of the vector q only, and $N(q, \dot{q})$ is a 4×1 vector comprised of elements of both q and its first derivative. Compared to the nonlinear dynamical model of serial robots, the matrix $M(q)$ is known as the inertia matrix and the vector $N(q, \dot{q})$ is the nonlinear term from Coriolos/centrifugal effects.

Substituting Eq. (12) into (3) is straightforward but requires significant space to show all the equations. Due to this reason, not all the details are included here. For reader's information, MAPLE software is used for taking derivatives and finding the matrices $M(q)$ and $N(q, \dot{q})$:

$$\frac{\partial L}{\partial \dot{d}} = 0,$$

$$\frac{\partial L}{\partial \dot{\theta}} = \frac{1}{2} I_x \dot{\theta},$$

$$\frac{\partial L}{\partial \dot{q_1}} = \rho A \dot{q_1} \int_0^{l-d} \varphi_1^2(y)dy + \rho A \dot{q_2} \int_0^{l-d} \varphi_1(y)\varphi_2(y)dy,$$

$$\frac{\partial L}{\partial \dot{q_2}} = \rho A \dot{q_2} \int_0^{l-d} \varphi_2^2(y)dy + \rho A \dot{q_1} \int_0^{l-d} \varphi_1(y)\varphi_2(y)dy,$$

$$\begin{aligned}\frac{\partial L}{\partial d} = \frac{\partial}{\partial d}\Bigg(&\frac{1}{2}\rho A \dot{q}_1^2 \int_0^{l-d} \varphi_1^2(y)dy + \frac{1}{2}\rho A \dot{q}_2^2 \int_0^{l-d} \varphi_2^2(y)dy \\ &+ \rho A \dot{q}_1 \dot{q}_2 \int_0^{l-d} \varphi_1(y)\varphi_2(y)dy - \frac{1}{2} E I_y q_1^2 \int_0^{l-d} (\varphi_1'')^2 dy \\ &- \frac{1}{2} E I_y q_2^2 \int_0^{l-d} (\varphi_2'')^2 dy - E I_y q_1 q_2 \int_0^{l-d} \varphi_1'' \varphi_2'' dy - \frac{1}{2} k_a q_1^2 \int_0^{l-d} \varphi_1^2(y)dy \\ &- \frac{1}{2} k_a q_2^2 \int_0^{l-d} \varphi_2^2(y)dy - k_a q_1 q_2 \int_0^{l-d} \varphi_1(y)\varphi_2(y)dy\Bigg),\end{aligned}$$

$$\frac{\partial L}{\partial \theta} = 0,$$

$$\frac{\partial L}{\partial q_1} = -EI_y q_1 \int_0^{l-d} (\varphi_1'')^2 dy - EI_y q_2 \int_0^{l-d} \varphi_1'' \varphi_2'' dy - k_a q_1 \int_0^{l-d} \varphi_1^2(y) dy$$
$$- k_a q_2 \int_0^{l-d} \varphi_1(y)\varphi_2(y) dy,$$
$$\frac{\partial L}{\partial q_2} = -EI_y q_2 \int_0^{l-d} (\varphi_2'')^2 dy - EI_y q_1 \int_0^{l-d} \varphi_1'' \varphi_2'' dy - k_a q_2 \int_0^{l-d} \varphi_2^2(y) dy$$
$$- k_a q_1 \int_0^{l-d} \varphi_1(y)\varphi_2(y) dy,$$

$$\frac{d}{dt}\left(\frac{\partial L}{\partial \dot{d}}\right) = 0,$$
$$\frac{d}{dt}\left(\frac{\partial L}{\partial \dot{d}}\right) = \frac{1}{2} I_x \ddot{\theta},$$
$$\frac{d}{dt}\left(\frac{\partial L}{\partial \dot{q}_1}\right) = \rho A \ddot{q}_1 \int_0^{l-d} \varphi_1^2(y) dy + \rho A \ddot{q}_2 \int_0^{l-d} \varphi_1(y)\varphi_2(y) dy,$$
$$\frac{d}{dt}\left(\frac{\partial L}{\partial \dot{q}_2}\right) = \rho A \ddot{q}_2 \int_0^{l-d} \varphi_2^2(y) dy + \rho A \ddot{q}_1 \int_0^{l-d} \varphi_1(y)\varphi_2(y) dy.$$

Therefore, the Lagrangian equation corresponding to the variable d is as follows:

$$-\frac{\partial}{\partial d}\left(\frac{1}{2}\rho A \dot{q}_1^2 \int_0^{l-d} \varphi_1^2(y) dy + \frac{1}{2}\rho A \dot{q}_2^2 \int_0^{l-d} \varphi_2^2(y) dy + \rho A \dot{q}_1 \dot{q}_2 \int_0^{l-d} \varphi_1(y)\varphi_2(y) dy\right.$$
$$- \frac{1}{2} EI_y q_1^2 \int_0^{l-d} (\varphi_1'')^2 dy - \frac{1}{2} EI_y q_2^2 \int_0^{l-d} (\varphi_2'')^2 dy - EI_y q_1 q_2 \int_0^{l-d} \varphi_1'' \varphi_2'' dy$$
$$- \frac{1}{2} k_a q_1^2 \int_0^{l-d} \varphi_1^2(y) dy - \frac{1}{2} k_a q_2^2 \int_0^{l-d} \varphi_2^2(y) dy$$
$$\left. - k_a q_1 q_2 \int_0^{l-d} \varphi_1(y)\varphi_2(y) dy\right) = f.$$

Similarly, the second Lagrangian equation is

$$\frac{1}{2} I_x \ddot{\theta} = \tau.$$

The third and fourth are

$$\rho A \ddot{q}_1 \int_0^{l-d} \varphi_1^2(y) dy + \rho A \ddot{q}_2 \int_0^{l-d} \varphi_1(y)\varphi_2(y) dy + EI_y q_1 \int_0^{l-d} (\varphi_1'')^2 dy$$
$$+ EI_y q_2 \int_0^{l-d} \varphi_1'' \varphi_2'' dy + k_a q_1 \int_0^{l-d} \varphi_1^2(y) dy + k_a q_2 \int_0^{l-d} \varphi_1(y)\varphi_2(y) dy = 0,$$

$$\rho A\ddot{q}_2 \int_0^{l-d} \varphi_2^2(y)dy + \rho A\ddot{q}_1 \int_0^{l-d} \varphi_1(y)\varphi_2(y)dy + EI_y q_2 \int_0^{l-d} (\varphi_2'')^2 dy$$
$$+ EI_y q_1 \int_0^{l-d} \varphi_1''\varphi_2''dy + k_a q_2 \int_0^{l-d} \varphi_2^2(y)dy + k_a q_1 \int_0^{l-d} \varphi_1(y)\varphi_2(y)dy = 0.$$

It was mentioned previously that the resulting dynamic equations will not include friction forces. In the flexible needle-soft tissue system, friction plays a significant role. In order to make the dynamic equation (13) represent a more accurate model of the system, it is important to at least approximately model friction and include it in the dynamics. Therefore, the complete dynamics of the system will be expressed as

$$M(q)\ddot{q} + N(q, \dot{q}) = F - F_f. \tag{14}$$

Due to the fact that friction always acts against the movement, it has appeared with a negative sign on the right-hand side. Possible models for friction are discussed later.

Overall, our proposed dynamic model consists of two types of parameters. One group is related to measurable physical properties such as E, I_y, ρ and A. Thanks to a physics-based approach to dynamic modeling, which readily incorporates known (or easily measurable) physical parameters such as Young's modulus of the needle. Another group of parameters relate to the tissue model and the needle/tissue friction force model, which can be estimated by collecting experimental data and using common system identification methods. This will be discussed later.

In summary, the Lagrangian formulation for a dynamic system comprising a moderately flexible needle in soft tissue in (12) was rearranged in the form of the generic dynamics of a robot by defining an appropriate state vector. Similar to robotic systems, the mass matrix $M(q)$ turns out to be a symmetric matrix in its dependence on the flexible needle's physical parameters. The structure of this matrix is reported below.

$$M = \begin{bmatrix} M_{11} & 0 & 0 & 0 \\ 0 & M_{22} & 0 & 0 \\ 0 & 0 & M_{33} & M_{34} \\ 0 & 0 & M_{43} & M_{44} \end{bmatrix}.$$

Also, the matrix $N(q, \dot{q})$ has the following structure:

$$N(q, \dot{q}) = \begin{bmatrix} 0 \\ 0 \\ N1(q, \dot{q}) \\ N2(q, \dot{q}) \end{bmatrix}.$$

From the physical behavior of the system, one may expect the state variables d and θ to evolve in time independently from those states that relate to the needle

deflection, i.e., q_1 and q_2. This expectation is reinforced by the vector $N(q, \dot{q})$ in which the first two elements are equal to zero. However, in our simulations, we see a negligible yet nonzero dependence of the trajectory for d on the initial values of q_1 and q_2. This deviation may be coming from the approximation of deflection with only two dominant shape modes.

On the other hand, q_1 and q_2 are related only to the state d which is in the direction of needle insertion. This means that the initial needle deflection changes during needle insertion (even though we have not considered tip effects in the dynamic model). Simulation results at the end of this paper will provide more description of this issue.

In the next section, parametric system identification methods used for both tissue model and needle/tissue friction force are presented.

3.2.2. *Parameter identification*

3.2.2.1. Least squares parameter estimation

Least squares parameter estimation is an optimization procedure for minimizing the squared discrepancies (errors) between data obtained by measurement and their expected values. In the context of a regression problem, the variation in a dependent variable, X, leads to changes in another variable, Y, where $Y = h(X) +$ white noise. The regression function h maps the two sampled data variables to each other, and is to be estimated from n pairs of data points (X_i, Y_i). Assume that the value of the function h is known in n data points $h(X_i)$, $i = 0, 1, \ldots, n$, and that $h(X_i) = x_{i1}\beta_1 + \cdots + x_{ip}\beta_p$. The least squares method provides a computationally convenient fit of this linear regression model to the experimentally obtained data points. The least squares estimates β_i are as follows when the n sampled data points are arranged in a matrix framework[29]:

$$\hat{\beta}_i = (X^T X)^{-1} X^T Y.$$

An extension of linear regression is called "weighted least squares". In this method, instead of minimizing the sum of squares, a weighted sum of squares of errors is minimized. An ordinary regression calculates the parameters based on the assumption that the white noise has a fixed variance. In real experimental data, various input/output measurements may experience various levels of noise. Such an inconsistency in the magnitude of noise (heteroskedasticity) makes the estimation no longer optimal. In input/output channels where the noise is not small, that portion of information should be weakened using a weight matrix W. Parameter estimation in the weighted least squares method follows

$$\hat{\beta}_i = (X^T W^{-1} X)^{-1} X^T W^{-1} Y.$$

This formulation is used later in this paper for both needle/tissue friction model estimation and tissue stiffness model identification.

3.2.2.2. Needle/tissue friction modeling and identification

The needle/tissue friction model is a component of the dynamic model that needs to be identified and incorporated into the Lagrangian dynamics (14). Recently, various studies have tried to model the friction force in percutaneous procedures.[30] Given the complex nature of friction, it is common to only consider its dominant terms. In the analysis of a dynamic system, a complex model of friction is rather uninformative. A simple model is *viscous friction* in which the friction force f_v is proportional to the needle insertion velocity $\dot{d}$ as $f_v = \mu_v \dot{d}$ where μ_v is the viscous friction constant. Another simple model is *Coulomb friction* f_s, which is constant except for a sign dependence on the insertion velocity as $f_s = \mu_s \operatorname{sign}(\dot{d})$ where μ_s is the Coulomb friction constant. A reasonable and simple model is to include both of these terms as

$$f_f = \mu_s \operatorname{sign}(\dot{d}) + \mu_v \dot{d} = f_s + f_v. \tag{15}$$

Thus, the vector form of friction term in (15) can be added to the other dynamic terms derived from the energy equations as

$$M(q)\ddot{q} + N(q, \dot{q}) = F - \begin{bmatrix} \mu_s \operatorname{sign}(\dot{d}) \\ 0 \\ 0 \\ 0 \end{bmatrix} - \begin{bmatrix} \mu_v \dot{d} \\ 0 \\ 0 \\ 0 \end{bmatrix}. \tag{16}$$

To further complete the dynamic model of the flexible needle in soft tissue, the friction coefficients μ_s and μ_v need to be estimated. To do so, an experiment is set up as described in the following. It is clear that during the time that the needle is moving through tissue, a cutting force exists at the tip of the needle in addition to the friction along the needle's length. In our modeling, this cutting force is neglected. To be able to ignore this cutting force and deal only with the friction force in (15), we collect experimental data when the needle tip has completely passed through the tissue. Then, we begin to apply an insertion force f_y, starting from zero and increasing it by small increments, until the needle starts to move; at this point, the force at the needle's base has just passed the Coulomb friction level. The needle's base force measurement data stored after this point corresponds to the sum of Coulomb friction and viscous friction. Meanwhile, the position and velocity of the needle's base, which is fixed to the robot, are read from the robot while a JR3 force sensor (JR3, Inc., Woodland, CA, USA) records the needle base forces. This data is collected from several experiments. Applying linear regression estimation to this data will give us an estimation of μ_s and μ_v.

Following the procedure stated above and by repeating the experiment 20 times, average values and standard deviations (STD) of Coulomb and viscous friction coefficients for a prostate implant needle (Model number 102482, World Wide Medical Technologies) were obtained. These are reported in Table 1. Figure 2 shows a sample profile of the needle base force measurement in the needle insertion experiment.

Table 1. Friction coefficient estimation.

Standard deviation and typical values for friction coefficients in 20 experiments	
Mean ± STD for μ_s	Mean ± STD for μ_v
0.56 ± 0.0374	0.3 ± 0.0447

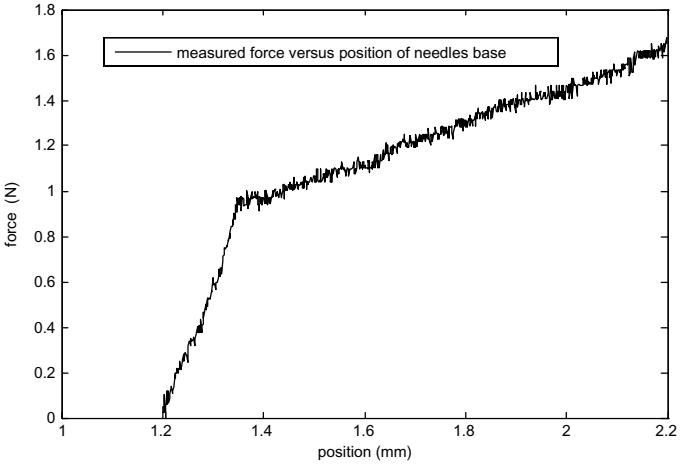

Fig. 2. Needle base force profile recorded for friction model identification. Needle was initially passed through the tissue to eliminate cutting forces.

3.2.2.3. Tissue model identification

The tissue model that we will be identifying later based on certain force/displacement measurements is in the form of a stiffness matrix. An important question that arises is, are our experimentally obtained force/displacement measurements describing a spring? A significant characteristic of a linear spring is that it stores elastic energy; the time integral of force times displacement is zero over a closed contour. In a general spring, force is an explicit function of position as $F = F(x)$. Therefore, the potential function related to the elastic energy is defined as

$$E_p(\mathbf{x}) = \int -\mathbf{F}^T d\mathbf{x}$$

or

$$\mathbf{F}(\mathbf{x}) = -\text{grad}_{\boldsymbol{x}} E_p(\mathbf{x}),$$

where $\text{grad}_{\boldsymbol{x}}$ represents the gradient with respect to $\mathbf{x}$ and the bold symbols denote vectors. In Cartesian coordinates, the position and force vectors are

$$\mathbf{x} = \begin{bmatrix} x \\ y \end{bmatrix}, \quad \mathbf{F} = \begin{bmatrix} F_x(x,y) \\ F_y(x,y) \end{bmatrix}, \quad -\text{grad}_{\boldsymbol{x}} E_p(x,y) \triangleq \begin{bmatrix} \dfrac{-\partial E_p}{\partial x} \\ \dfrac{-\partial E_p}{\partial y} \end{bmatrix} = \begin{bmatrix} F_x(x,y) \\ F_y(x,y) \end{bmatrix}.$$

The curl of the vector field $\mathbf{F}$ is defined as

$$\operatorname{curl}\mathbf{F}(x,y) = \frac{\partial F_x}{\partial y} - \frac{\partial F_y}{\partial x},$$

which is directly related to the mechanical work required for movement. A sufficient and necessary condition for spring-like behavior of a system is to have a vector field with zero curl, which is equivalent to having a conservative force field.[30]

If a vector field is nonlinear but differentiable around an operating point, then a Taylor series expansion might be used for it. For sufficiently small displacements, high order terms in the series can be neglected, resulting in the following first-order relation between the force and displacement vectors:

$$\begin{bmatrix} F_x \\ F_y \end{bmatrix} = \begin{bmatrix} -k_{xx} & -k_{xy} \\ -k_{yx} & -k_{yy} \end{bmatrix} \begin{bmatrix} d_x \\ d_y \end{bmatrix},$$

$$-k_{xx} = \frac{\partial F_x}{\partial x}, \quad -k_{xy} = \frac{\partial F_x}{\partial y},$$

$$-k_{yx} = \frac{\partial F_y}{\partial x}, \quad -k_{yy} = \frac{\partial F_y}{\partial y}.$$

The above relationship defines a stiffness matrix. In a pure spring, the stiffness matrix is symmetric:

$$-k_{xy} = \frac{\partial F_x}{\partial y} = \frac{\partial F_y}{\partial x} = -k_{yx}.$$

Otherwise, the stiffness matrix is not symmetric.

We are interested in a metric that determines how closely a given 2D stiffness matrix resembles an actual spring. The 2D stiffness matrix can be decomposed into two parts: a symmetric matrix and an anti-symmetric (skew-symmetric) matrix. This decomposition is formulated as

$$k_{2\times 2} = \underbrace{\frac{1}{2}(k + k^T)}_{\text{symmetric term}} + \underbrace{\frac{1}{2}(k - k^T)}_{\text{anti-symmetric term}}.$$

The symmetric matrix represents forces that correspond to the elastic energy function. Since the force–displacement relation is a vector field, the curl of this field is a vector operator that describes the infinitesimal rotation of a field. The symmetric component of the stiffness matrix has a zero curl while the anti-symmetric component possesses a nonzero curl. If the curl of the anti-symmetric part is small enough, the total stiffness matrix can be assumed to describe an actual spring; this will speak to the validity (or lack thereof) of an identified spring model.

To test the validity of the spring model for our soft tissue, it is only necessary to make a small displacement around an equilibrium point by applying a small force using an indenter (e.g., a robot end-effector) to the tissue. For this small displacement, the force–displacement relation of the tissue can be considered linear. To find the tissue stiffness coefficient denoted by k_a in (8), we apply forces to the tissue in

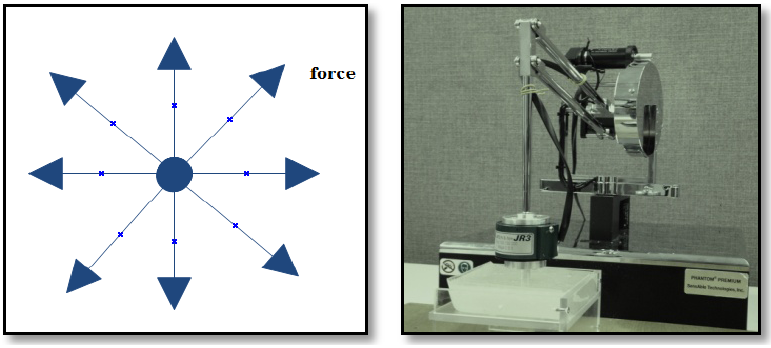

Fig. 3. (Left) Eight directions of applied force in the tissue identification experiment. (Right) Experimental test-bed for tissue identification.

eight directions as depicted in Fig. 3. We place the robot end-effector in the center of our phantom tissue[a] to avoid inaccuracies introduced by boundary conditions between the tissue edges and the container that holds the tissue. The stiffness coefficient of tissue, which is assumed to be homogeneous, can be estimated by the least squares method using measurements of applied forces and their corresponding tissue displacements. Forces are applied in two dimensions (in the plane of needle deflection), which lead to a 2×2 stiffness matrix. However, in the needle/tissue dynamics, we need only one element of this matrix, corresponding to the stiffness along the needle deflection direction, k_{zz} (see Fig. 1).

Having identified the tissue stiffness coefficient as described above, the mean and standard deviation of measured values of the tissue stiffness are reported in Table 2. This experiment was run 20 times in different tissue locations. From this table, the consistency of estimated stiffness is evident from the small values of STD for both k_{xx} and k_{zz}. From these experiments, k_a was found to be $0.52\,\mathrm{kN/m^2}$ when the applied force was 1.5 N in magnitude. Our results confirm the reliability of this

Table 2. Tissue stiffness identification statistical numbers.

	Applied forces are in Newton									
	$f = 1.1$		$f = 1.2$		$f = 1.3$		$f = 1.4$		$f = 1.5$	
	mean	STD	mean	STD	mean	STD	mean	STD	mean	STD
$\boldsymbol{k_{xx}}$	1.26	0.08	0.82	0.54	1.10	0.11	1.03	0.12	0.96	0.12
$\boldsymbol{k_{zz}}$	1.01	0.11	0.81	0.15	0.69	0.18	0.60	0.19	0.52	0.18
$\boldsymbol{k_{xz}}$	0.04	0.08	0.04	0.07	0.01	0.09	0.001	0.08	−0.005	0.08
$\boldsymbol{k_{zx}}$	−0.10	0.06	−0.10	0.10	−0.11	0.09	−0.11	0.09	−0.11	0.09

[a]This phantom tissue is made of 75% liquid plastic with 25% plastic softener from M-F manufacturing Co.

spring model for the phantom tissue under consideration. As expected, the anti-symmetric part has small curl with the average values of k_{xy} and k_{yx} reported in Table 2. This means that the spring model does capture the input–output behavior of the tissue well. Due to some off-plane movements of the robot's end effector in the x-direction, for the bigger applied forces, k_{xx} values are not close to the k_{zz} values, as expected for a homogeneous tissue.

In both identification procedures for the tissue model and the friction model, data were first low-pass filtered to attenuate high frequency noise coming from the force sensor.

3.2.3. *Analysis of the dynamical system*

Before designing a controller for an open-loop system, the system controllability must be investigated to determine whether there exists an input signal that can force the system from an initial state into a particular desired state. To look at the controllability of the needle/tissue system with the dynamics given in (16), the state space representation of the system is required. Let us rewrite the system equation as

$$\ddot{q} = M^{-1}(q)(F - N'(q, \dot{q})), \tag{17}$$

where $N'(q, \dot{q}) = F_v + N(q, \dot{q}) + F_s$. By defining the state vector

$$\begin{aligned} X = [X_1 \quad X_2]^T &= [x_1 \quad x_2 \quad x_3 \quad x_4 \quad x_5 \quad x_6 \quad x_7 \quad x_8]^T \\ &= [d \quad \theta \quad q_1 \quad q_2 \quad \dot{d} \quad \dot{\theta} \quad \dot{q}_1 \quad \dot{q}_2]^T, \end{aligned}$$

the state space representation of the flexible needle-soft tissue system is given as

$$\dot{X} = \begin{bmatrix} x_5 \\ x_6 \\ x_7 \\ x_8 \\ -M^{-1}(X_1)\acute{N}(X_1, X_2) \end{bmatrix} + \begin{bmatrix} 0 \\ 0 \\ 0 \\ 0 \\ M^{-1}(X_1)(F) \end{bmatrix}. \tag{18}$$

The output equation for the deflection of the needle's tip is

$$Y = w(l - d, t) = q_1(t)\varphi_1(l - d) + q_2(t)\varphi_2(l - d).$$

3.2.4. *Linearization of the nonlinear system*

In needle insertion, it is quite reasonable to assume that the surgeon or the robotic system applies small changes in inputs. Thus, we only need to study the controllability of the linearized system around an operating point instead of that of the nonlinear system. The linearization of the general nonlinear system

$$\dot{X} = f(X) + \sum_{i=1}^{m} g_i(X)u_i, \quad Y = h(X, U),$$

(where X, Y and U are the state, the output and the input vectors, respectively) around X_0 and U_0 is

$$\begin{cases} \dot{X} = AX + BU \\ Y = CX + DU \end{cases}. \tag{19}$$

In the above,

$$A = \left.\frac{\partial f(X)}{\partial X}\right|_{X_0} + \left.\sum_{i=1}^{m} \frac{\partial g_i(X)}{\partial X} u_i\right|_{X_0,U_0}, \quad B = \left.\sum_{i=1}^{m} \frac{\partial g_i(X) u_i}{\partial u_i}\right|_{X_0},$$

$$C = \left.\frac{\partial h(X,U)}{\partial X}\right|_{X_0}, \quad D = \left.\frac{\partial h(X,U)}{\partial U}\right|_{X_0}.$$

For a nonlinear system, the linearized system relates to a nominal input as well as nominal states. Therefore, verification of the controllability, observability and other possible features of the nonlinear system are only valid around the particular operating point of the states and the input.

Based on (18) and (19) and for the operating point $[d_0 \ \theta_0 \ 0 \ 0 \ \dot{d}_0 \ \dot{\theta}_0 \ 0 \ 0]^T$, the linearized model is given by

$$A = \begin{bmatrix} 0_{4\times4} & I_{4\times4} \\ \left.\frac{\partial(-M^{-1}(X_1)N'(X_1,X_2))}{\partial X_1} + \frac{\partial M^{-1}(X_1)F}{\partial X_1}\right|_{X_0} & \left.\frac{\partial(-M^{-1}(X_1)N'(X_1,X_2))}{\partial X_2}\right|_{X_0} \end{bmatrix}_{8\times8},$$

$$B = \begin{bmatrix} 0_{4\times2} \\ \left. M^{-1}(X_1) \times \begin{bmatrix} 1 & 0 \\ 0 & 1 \\ 0 & 0 \\ 0 & 0 \end{bmatrix} \right|_{X_0} \end{bmatrix}_{8\times2},$$

$$C = \left[\left.\frac{\partial(x_3\varphi_1(l-x_1) + x_4\varphi_2(l-x_1))}{\partial X}\right|_{X_0}\right]_{1\times8}, \quad D = 0_{1\times2},$$

in which $I_{4\times4}$ is the identity matrix.

We can now study the behavior of the linearized system around a couple of operating points for the state vector X.

3.2.5. *Controllability analysis*

Definition. A system is output controllable in a period (t_0, t_l) if for any given t_0 and t_l, any final output at t_l can be achieved starting with arbitrary initial conditions in the system at t_0. A system is state controllable in a period (t_0, t_l) if for any given t_0 and t_l, any final state at t_l can be achieved starting with arbitrary initial conditions in the system at t_0.

It has been shown that a linear system described by matrices A, B, C and D is output controllable if and only if the output controllability matrix $Q_{m\times mn}$

$$Q = [CB \quad CAB \quad \dots \quad CA^{n-1}B \quad D],$$

has rank m where m is the number of inputs and n is the number of the state variables. Similar to the output controllability, state controllability is satisfied if and only if the controllability matrix $\mu_{n\times mn}$

$$\mu_{n\times mn} = [B \quad AB \quad A^2B \quad \cdots \quad A^{n-1}B],$$

is full rank. A state controllable system is not necessarily output controllable and vice versa.

For the linearized system (19), it is found that the needle-tissue system is fully controllable around some of the operating points while for some others there is a deficiency in the rank of the controllability matrix. In contrast, the output controllability condition is not satisfied for most of the operating points, which means that the inputs defined for the system are not able to influence the needle's tip deflection in a desired way. This result was expected as in manual needle insertion it is normally observed that f_y and τ in Fig. 1 are inadequate for maneuvering the needle; in practice, the surgeon needs to apply a lateral force as well or rotate the needle around the y-axis to use the bevel-tip angle for properly controlling the needle.

3.2.6. *Observability analysis*

For designing a state feedback controller, the states of the system are assumed to be available. Aside from a control point of view, the knowledge of the states of the system is required for fault monitoring and detection purposes. In practice, the entire vector of states is rarely available because having each state is equivalent to having a physical sensor. In addition to the fact that sensors increase the cost of the control system, in some cases a sensor cannot be mounted in the proper location and some of the states may not even correspond to physical signals. For these reasons, we need to reconstruct the state information from other measurable input and output data. In this case, under some conditions — namely when the system is observable — an observer can be used to estimate the states. Although designing an observer for linear time-invariant systems is well formulated, the same problem for nonlinear systems is challenging.

Definition. A system is said to be observable if for any initial state X_0 and fixed time $t_1 > 0$, the knowledge of the input u and output Y over $[0, t_1]$ suffices to determine the initial state X_0 uniquely. Once the initial state is determined, any state at time t_1 can be reconstructed from the dynamic equation of the system. The linear time-invariant system with state, input and output matrices A, B and C is observable if and only if the observability matrix

$$O_{n\times mn} = [C \quad CA \quad CA^2 \quad \cdots \quad CA^{n-1}]^T,$$

has a full rank.

Analyzing the linearized needle-tissue system in (19), it is found that while there is a rank deficiency of 2 in the observability matrix, those states that are not physically measurable, q_1 and q_2, are observable.

3.2.7. *Controller design*

3.2.7.1. Inverse dynamic control

If the dynamics of a system is fully given as in (17), an inverse dynamics controller becomes an option. For the dynamic system in (17), the inverse dynamics controller is given by

$$F_c = M(q)(\ddot{q}_d + k_v\dot{q}_e + k_p q_e) + \acute{N}(q, \dot{q}),$$
$$\dot{q}_e \triangleq \dot{q}_d - \dot{q},$$
$$q_e = q_d - q,$$

where F_c is the controller output vector, q_d is the desired state vector, and k_v and k_p are the controller gain matrices related to the velocity and position, respectively. The controller matrix gain k_v and k_p should be chosen as positive definite matrices for the sake of stability of the closed-loop system. The closed-loop system dynamics will be

$$\ddot{q} = \ddot{q}_d + k_v\dot{q}_e + k_p q_e.$$

By choosing positive definite matrices for k_v and k_p, the state error q_e and its derivative $\dot{q}_e$ will converge to zero. Later, the simulation results for this inverse dynamics controller are reported.

3.2.7.2. Proportional-Integral-Derivative (PID) control

Among non-model-based controllers, PID is famous for its reliable and robust results. Here, we optimize the proportional, integral and derivative terms of the controller by trial and error to get minimum needle deflection. Understandably, the main issue with this controller is that adjusting its gains does not follow a general rule and it varies from one dynamic model to another.

The next session compares the simulation results for the PID and inverse dynamic controllers.

3.2.8. *Simulation results*

In the following, let us consider a reduced dynamic model of the system in order to verify the effect of the insertion force f_y on the needle tip deflection. To this end, the input torque (needle rotation around its length axis) is not applied and therefore, the second state variable θ and its corresponding torque input τ are not considered. Accordingly, all matrix dimensions in (14) reduce from order 4 to order 3. For all simulation results, the desired vector q_d is set to zero (ideally zero deflection) when the needle is fully inserted into soft tissue.

Table 3. Physical system parameters.

Parameter		Values are for an 18 gauge flexible needle[a]	
		Value	Unit
E	Young's modulus	200	G pa
I_y	Cross-sectional moment of inertia	1.28×10^{-13}	m^4
I_x	Cross-sectional moment of inertia	1.0626×10^{-9}	m^4
ρ	Density	8000	kg/m^3
A	Effective cross-sectional area	1.27×10^{-6}	m^2
l	Needle's effective length	0.2	m
g	Gravity constant	9.89	m/s^2

[a]Model number 102482, World Wide Medical Technologies.

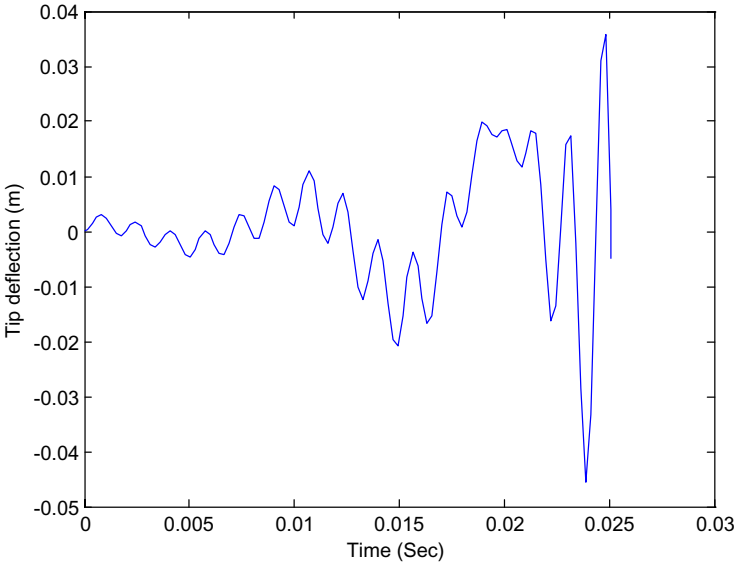

Fig. 4. Needle tip's deflection in the open-loop model.

Table 3 shows the physical parameter values corresponding to the 18-gauge needle in our setup.

Figures 4 and 5 are the simulated responses to an input force equal to 3 N with the needle initially inserted 2 cm in the tissue with an initial deflection of 0.5 mm. For the simulation, the average values reported in Table 1 are used for the friction model. Also, the stiffness coefficient of the phantom tissue is set to $0.52\,kN/m^2$ as calculated. From Fig. 4, it is concluded that the needle tip's deflection varies as the needle passes through the tissue.

Figures 6 and 7 show the needle tip's deflection and the states of the closed-loop system under the inverse dynamic controller, respectively. For inverse dynamic

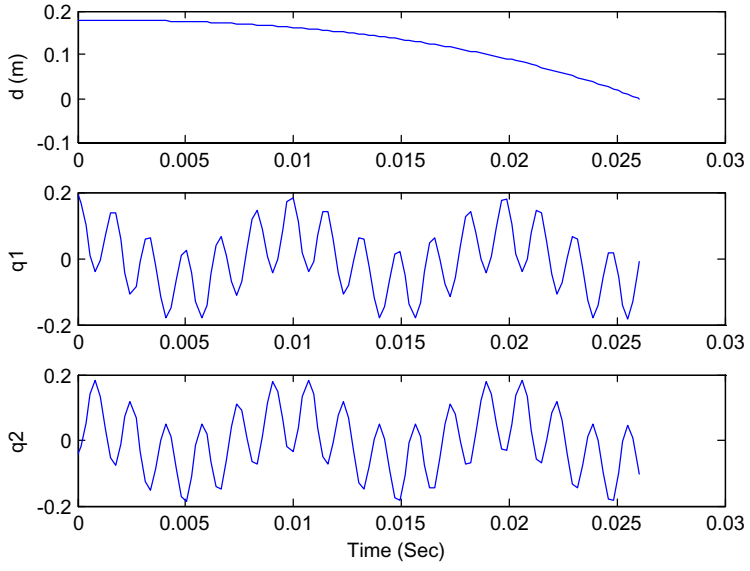

Fig. 5. State variables of the open-loop system.

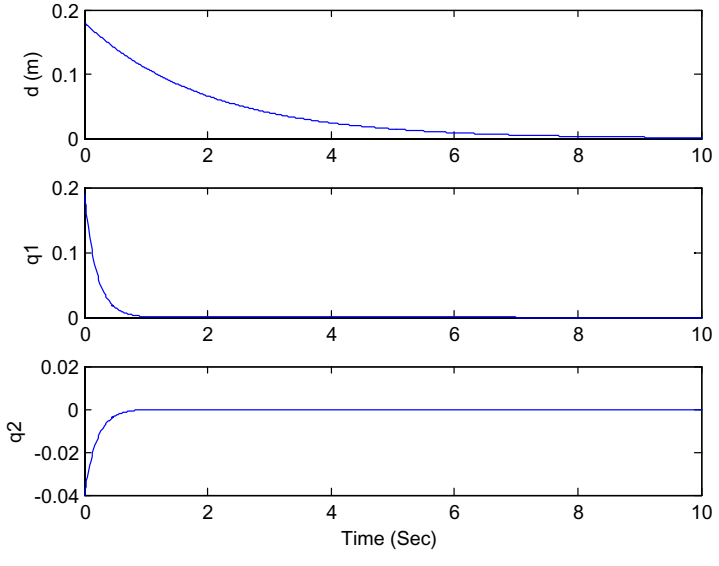

Fig. 6. State variables in the closed-loop system under inverse dynamics control.

controller, the matrix gains are chosen diagonal as

$$k_p = \text{diag}\{[1 \quad 10 \quad 10]\},$$
$$k_v = 0.1\, k_p.$$

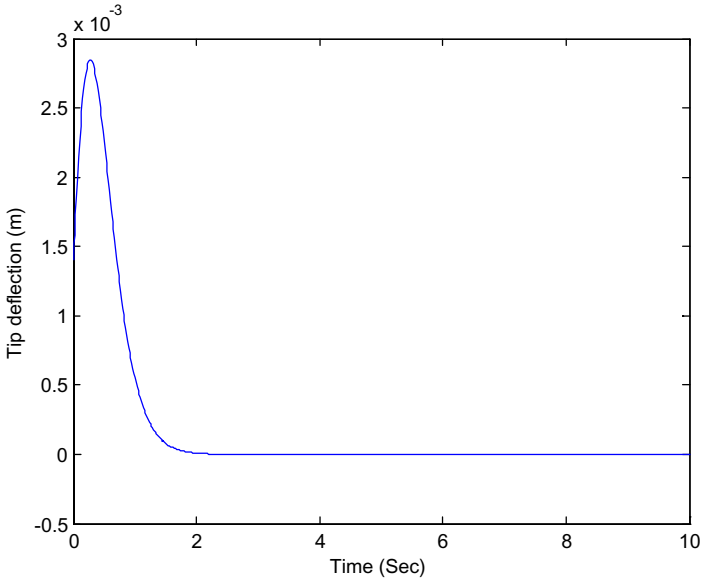

Fig. 7. Needle tip's deflection in the closed-loop system under inverse dynamics control.

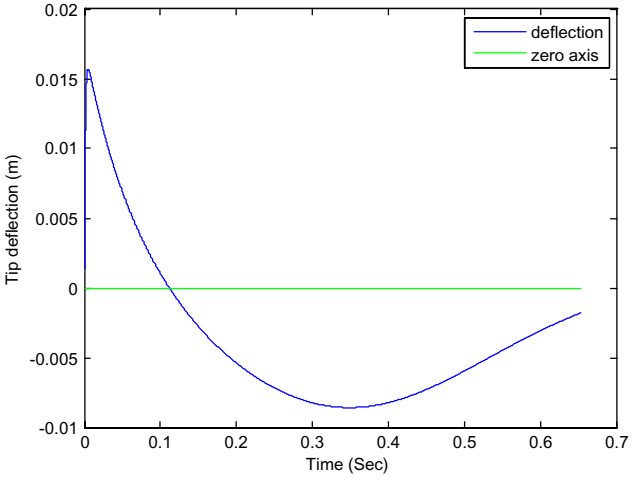

Fig. 8. Needle tip's deflection in the closed-loop system under PID control.

Also, the PID controller's results are depicted in Fig. 8. For this controller, minimum needle deflection is resulted by applying the following gain matrices:

$$k_p = 10^3 \times \mathrm{diag}\{[1 \quad 1 \quad 1]\},$$
$$k_v = 10\, k_p.$$

In general, closed loop controlled system provides smoother response in needle tip deflection. A comparison between the results of the inverse dynamic controller with the PID controller reveals that the former leads to zero deflection as time grows whereas the PID controller results in a nonzero position error, which is not desired. Therefore, as we expected, the controller which is informed by the dynamic model of the system, can better make the needle tip follow a desired trajectory. Nonetheless, it must be noted that in reality we will not have a zero tip positioning error due to the existence of noise and inevitable open-loop model identification inaccuracies.

3.2.9. *Conclusion and future study*

Recent studies on steering flexible needles in soft tissue attempt to employ computer-controlled steering in order to achieve more precise needle positioning. This aim may not be achievable without a complete understanding of the dynamic behavior of the needle/tissue system. This motivates deriving dynamical equations governing a flexible needle in soft tissue. This paper explained the derivation of the dynamic model of a coupled needle/tissue system based on the Lagrangian formulation. The significance of this model is that it is physics-based and includes both the needle's elasticity parameters such as Young's modulus and the model of tissue deformation. This model does not consider unbalanced forces coming from the needle's bevel tip. We considered the effect of needle/tissue friction in the dynamic model. The least squares estimation method was used for identifying the parameters of tissue and friction models. Steerability (controllability) and observability analyses of the linearized system was done; the results for selected operating points confirm the controllability of this dynamic system. Simulation results show that the initial needle deflection can be a cause of further needle deflection during insertion. Moving forward, having a dynamic model of the flexible needle in soft tissue, we implemented two controllers: an inverse dynamics controller and a PID controller. Simulation results confirmed that knowing the dynamical properties of an open-loop system helps to get a better performance in the closed-loop system.

For future study, one can consider the effect of needle tip type (bevel, trocar) in the dynamic model. An alternative approach for the model-based control strategy would be to design an adaptive controller, given that the tissue and the needle cannot be modeled precisely. In fact, control methodologies that ensure robustness are welcome additions as there will always be uncertainties in the modeling due to variations in tissue structures and needle parameters.

Acknowledgment

Research supported in part by the Natural Sciences and Engineering Research Council (NSERC) of Canada.

References

1. Taschereau R., Pouliot J., Roy J., Tremblay D., Seed misplacement and stabilizing needles in transperineal permanent prostate implants, *Radiother. Oncol.* **55**(1):59–63, 2000.
2. Nath S., Chen Z., Yue N., Trumpore S., Peschel R., Dosimetric effects of needle divergence in prostate seed implant using I and Pd radioactive seeds, *Med. Phys.* **27**:1058, 2000.
3. Al-Qaisieh B., Pre- and post-implant dosimetry: An intercomparison between UK prostate brachytherapy centres, *Radiother. Oncol.* **66**:181–183, 2003.
4. Dawson J. E., Wu T., Roy T., Gu J. Y., Kim H., Dose effects of seed placement deviations from pre-planned positions in ultrasound guided prostate implants, *Radiother. Oncol.* **32**:268–270, 1994.
5. Alterovitz R., Goldhere K., Pouliot J., Taschereau R., Hsu I. C., Needle insertion and radioactive seed implantation in Human tissues: Simulation and sensitivity analysis, in *Proc. IEEE Int. Conf. Robotics & Automation* (*ICRA*), Vol. 2, pp. 1793–1799, 2003.
6. DiMaio S. P., Salcudean S. E., Needle insertion modeling and simulation, *IEEE Trans. Robot. Autom.*, Special Issue Med Robotics, **19**:864–875, 2003.
7. Dehghan E., Salcudean S. E., Needle insertion parameter optimization for brachytherapy, *IEEE Trans. Robot.* **25**:509–525, 2009.
8. Doblare M. *et al.*, On modeling soft biological tissue with natural element method, *Int. J. Model., Simulat., Sci. Comput.* **87**:87–116, 2007.
9. Webster R. J. I., Kim J. S., Cowan N. J., Chirikjian G. S., Okamura A. M., Nonholonomic modelling of needle steering, *Int. J. Robot. Res.* **25**:509–525, 2006.
10. Alterovitz R., Branicky M., Goldberg K., Motion planning under uncertainty for image-guided needle steering, *Int. J. Robot. Res.* **27**(11–12):1361–1374, 2008.
11. Alterovitz R., Goldberg K., Okamura A., Planning for steerable bevel-tip needle insertion through 2D soft tissues with obstacles, *IEEE Int. Conf. Robotics and Automation*, pp. 1652–1657, 2005.
12. Park W., Kim J. S., Zhou Y., Cowan N. J., Okamura A. M., Chirikjian G. S., Diffusion-based motion planning for a nonholonomic flexible needle model, *IEEE Int. Conf. Robotics and Automation*, pp. 4600–4605, 2005.
13. DiMaio S. P., Modeling simulation and planning of needle motion in soft tissues, Ph.D. thesis, University of British Colombia, 2003.
14. Glozman D., Shoham M., Image-guided robotic flexible needle steering, *IEEE Trans. Robot.* **23**:459–466, 2007.
15. Yan K. G., Podder T., Xiao D., Yu Y., Liu T. I., Cheng C., An improved needle steering model with online parameter estimator, *Int. J. Comput. Assisted Radiol. Surg.* **1**:205–212, 2006.
16. Dehghan E., Goksel O., Salcudean S. E., A comparison of needle bending models, *Proc. Medical Image Computing and Computer Assisted Intervention* (*MICCAI*), pp. 305–312, 2006.
17. DiMaio S. P., Salcudean S. E., Needle steering and model-based trajectory planning, *Proc. Medical Image Computing and Computer-assisted Intervention* (*MICCAI*), pp. 33–40, 2003.
18. http://en.wikipedia.org/wiki/Hough_transform.
19. Haddadi A., Goksel O., Salcudeen S. E., Hashtrudi-zad K., On the controllability of dynamic model-based needle insertion in soft tissue, *Annual Int. Conf. IEEE, Engineering in Medicine and Biology Society* (*EMBC*), Buenos Aires, Argentina, pp. 2278–2291, 2010.

20. Lindsey Q. J., Tenenholtz N. A., Lee D. I., Kuchenbecker K. J., Image-enabled force feedback for robotic teleoperation of a flexible surgical tool, in *Proc. IASTED Int. Conf. on Robotics and Applications*, Vol. 644, No. 033, 2009.
21. Asadian A., Kermani M. R., Patel R. V., An analytical model for deflection of flexible needles during needle insertion, *IEEE/RSJ Int. Conf. Intelligent Robots and Systems* (*IROS*), San Francisco, CA, USA, pp. 2552–2556, 2011.
22. Fung R. F., Chang H. C., Dynamic modeling of a non-linearly constrained flexible manipulator with a tip mass by Hamilton's principle, *J. Sound Vib.* **16**:751–769, 1998.
23. Giachetta G., Mangiarotti L., Sardanashvili G. A., New Lagrangian and Hamiltonian methods in field theory: Chaps. 3 and 4, World Scientific Publishing Co. Pte. Ltd., Singapore, 1997.
24. Low K. H., Vidyasagar M., A Lagrangian formulation of the dynamic model for flexible manipulator systems, *ASME J. Dyn. Syst., Meas., Control* **110**:175–181, 1988.
25. Craig J. J., *Introduction to Robotics: Mechanics and Control*, 3rd edn., Pearson Education, Inc., p. 182, 2004.
26. Meirovitch L., Computational methods in structural dynamics, Vol. 5, Springer, 1980.
27. Wang D., Vidyagasar M., Transfer functions for a single flexible link, *Int. J. Robot. Res.* **10**(5):540–549, 1989.
28. Liu J. X., Robot Manipulators: New Research, Chap. 1, Nova Science Publishers Inc., New York, 2005.
29. Van De Geer S. A., Least squares estimation, in *Encyclopedia of Statistics in Behavioral Science*, Vol. 2, John Wiley & Sons, Ltd., Chichester, pp. 1041–1045, 2005.
30. Ivaldi M., Ferdinando A., Hogan N., Bizzi E., Neural, mechanical, and geometric factors subserving arm posture in humans, *J. Neurosci.* **5**:2732–2743, 1985.